The Journal of Chemical Physics

RESEARCH ARTICLE | DECEMBER 03 2018

Hyperfine-interaction-induced g/u mixing and its implication on the existence of the first excited vibrational level of the $A^+ {}^2\Sigma_u^+$ state of H_2^+ and on the scattering length of the H + H⁺ collision

Maximilian Beyer ; Frédéric Merkt

Check for updates

J. Chem. Phys. 149, 214301 (2018)
https://doi.org/10.1063/1.5046147

View Online Export Citation

Articles You May Be Interested In

Tetraneutron resonance: Theory
AIP Conf. Proc. (November 2018)

Semiclassical calculation for collision induced dissociation. II. Morse oscillator model
J. Chem. Phys. (February 1978)

Protonium formation in $\bar{p}$ + H(1*s*) collision
AIP Conf. Proc. (October 2005)

25 July 2026 18:11:09

AIP Advances
Why Publish With Us?
21DAYS average time to 1st decision
OVER 4 MILLION views in the last year
INCLUSIVE scope
Learn More
AIP Publishing

AIP Publishing

Hyperfine-interaction-induced g/u mixing and its implication on the existence of the first excited vibrational level of the $A^+\ ^2\Sigma_u^+$ state of H_2^+ and on the scattering length of the H + H^+ collision

Maximilian Beyer and Frédéric Merkt
Laboratorium für Physikalische Chemie, ETH Zürich, 8093 Zürich, Switzerland

(Received 26 June 2018; accepted 29 October 2018; published online 3 December 2018)

Ab initio calculations of the energy level structure of H_2^+ that include relativistic and radiative corrections to nonrelativistic energies and the diagonal part of the hyperfine interaction have predicted the existence of four bound rovibrational levels [(v = 0, N = 0 − 2) and (v = 1, N = 0)] of the first electronically excited ($A^+\ ^2\Sigma_u^+$) state of H_2^+, the (v = 1, N = 0) level having a calculated binding energy of only E_b = 1.082 219 8(4)·10^{-9} E_h and leading to an extremely large scattering length of 750(5) a_0 for the H^+ + H collision [J. Carbonell *et al.*, J. Phys. B: At., Mol. Opt. Phys. **37**, 2997 (2004)]. We present an investigation of the nonadiabatic coupling between the first two electronic states ($X^+\ ^2\Sigma_g^+$ and $A^+\ ^2\Sigma_u^+$) of H_2^+ induced by the Fermi-contact term of the hyperfine-coupling Hamiltonian. This interaction term, which mixes states of total spin quantum number G = 1/2, is rigorously implemented in a close-coupling approach to solve the spin-rovibronic Schrödinger equation. We show that it mixes states of gerade and ungerade electronic symmetry, that it shifts the positions of all weakly bound rovibrational states of H_2^+, and that it affects both the positions and widths of its shape resonances. The calculations demonstrate that the G = 1/2 hyperfine component of the A^+ (v = 1, N = 0) state does not exist and that, for G = 1/2, the s-wave scattering lengths of the H^+ + H(1s) collision are −578(6) a_0 and −43(4) a_0 for the F = 0 and F = 1 hyperfine components of the H(1s) atom, respectively. The binding energy of the G = 3/2 hyperfine component of the A^+ (v = 1, N = 0) state is not significantly affected by the hyperfine interaction and the corresponding scattering length for the H^+ + H(1s, F = 1) collision is 757(7) a_0. © *2018 Author(s). All article content, except where otherwise noted, is licensed under a Creative Commons Attribution (CC BY) license (http://creativecommons.org/licenses/by/4.0/).* https://doi.org/10.1063/1.5046147

25 July 2026 18:11:09

I. INTRODUCTION

The H^+ + H(1s) collision is the simplest reactive collision involving two identical fermions. It is a system of fundamental importance in atom scattering[1–5] and for the understanding of molecule formation in the universe.[6–11] Most treatments of this collision have disregarded the role of the hyperfine interaction and thus treated the collision assuming elastic scattering on the uncoupled potential curves of the ground $X^+\ ^2\Sigma_g^+$ and first excited $A^+\ ^2\Sigma_u^+$ electronic states. This approximation is excellent at collision energies that are much larger than the hyperfine splittings of H(1s) and of the rovibronic levels of H_2^+ but is expected to break down at very low temperatures, where the collision energies are comparable or smaller than the hyperfine splittings. At such low temperatures, the hyperfine interaction may manifest itself through two related qualitative changes compared to the hyperfine-interaction-free case: First, the common dissociation asymptote H^+ + H(1s) of the X^+ and A^+ states splits into two hyperfine components, separated by about 1400 MHz and corresponding to H^+ + H(1s, F = 0, 1). Second, the hyperfine interaction breaks the gerade/ungerade (g/u) (and also the ortho-para) symmetry and fully mixes the X^+ and A^+ states in the range of internuclear distances where the separation between the adiabatic potential curves of these states is less than the hyperfine interaction.

Both manifestations of the hyperfine interaction are well known and have been discussed in the literature. In their elegant measurements of transitions between weakly bound rovibrational levels of the X^+ and A^+ states by microwave spectroscopy, Carrington and co-workers observed unexpected line shifts and line splittings[12] that were interpreted by Moss[13] and Bunker and Moss[14] as arising from g/u-symmetry breaking. Later, McNab and co-workers observed a nominally forbidden pure rotational transition between the N = 0 and 1 rotational levels of the $X^+(v = 19)$ state of H_2^+[15] that was interpreted as being caused by the g/u-symmetry-breaking nature of the hyperfine interaction.[16]

The potential importance of the hyperfine interaction in the discussion of the possible existence of the very weakly (if at all) bound $A^+(v = 1, N = 0)$ state of H_2^+[17–19] was also recognized by Carbonell *et al.*,[20] who included the diagonal part of the hyperfine Hamiltonian in their nonadiabatic calculations in addition to relativistic and radiative corrections (see the four equations presented in Sec. 5 of their article). They came to the conclusion that the hyperfine interaction did not significantly modify the binding energy of the $A^+(v = 1, N = 0)$ state compared to an earlier calculation that disregarded the

 © Author(s) 2018

hyperfine interaction and relativistic and radiative corrections to the level energies.[19] The consequence of the weakly bound nature of the $A^+(v = 1, N = 0)$ state of H_2^+ is an extremely large s-wave scattering length for the $H^+ + H(1s)$ collision, which Carbonell *et al.*[19,20] found to be 750(5) a_0,[19,20] regardless of the inclusion or not of the hyperfine interaction in the theoretical treatment.

More recent theoretical investigations of the $H^+ + H(1s)$ collision at very low collision energies (or ultracold temperatures) essentially confirmed this large value of the scattering length. Bodo *et al.*,[4] who did not include the hyperfine interaction in their treatment, reported a value of 725 a_0. Li and Gao,[5] who stressed the importance of the hyperfine interaction in the $H^+ + H(1s)$ collision at low temperatures, calculated the scattering length to be 810.52 a_0. This value is in close agreement with the earlier values of 801.2 a_0 determined by Glassgold *et al.*[21] and of 762.8 a_0 determined by Kaiser *et al.*,[22] who, however, disregarded the hyperfine interaction. Li and Gao[5] also presented an elegant treatment of the g/u mixing induced by the hyperfine interaction based on multichannel quantum defect theory (MQDT). They determined the elastic and hyperfine-changing inelastic collision cross sections for the range between 0 and 5 K in MQDT calculations as well as using the coupled-channel numerical method, taking the hyperfine interaction to be independent of the internuclear separation. In the MQDT treatment, the hyperfine interaction is explicitly treated in the dissociation channels, neglected at short range, and its overall effect is obtained through a frame transformation, in analogy to the treatment of the hyperfine structure in Rydberg states of atoms[23] and molecules.[24]

This overview of previous determinations of the s-wave scattering length of the $H^+ + H(1s)$ collision leads to several puzzling conclusions: (i) The s-wave scattering length, which corresponds to the zero-energy limit of the collision, should be very sensitive to the hyperfine interaction, as discussed above. However, theoretical treatments that include and neglect the hyperfine interaction appear to yield very similar values for the scattering length. (ii) Although the g/u-symmetry-breaking role of the hyperfine interaction is widely recognized (see above), the large value of the s-wave scattering length appears to always be associated with the scattering length for ungerade electronic symmetry, although, strictly, it should be reported as the scattering length for the $F = 0$ hyperfine component of the H(1s) fragment.

The purpose of this article is to present the solution to these apparent contradictions, which we find are linked to the g/u-symmetry-breaking nature of the hyperfine interaction. g/u-symmetry breaking can also be induced by an external electric field, and a close-coupling calculation of this effect in H_2^+ was presented by Leach, Child, and Manolopoulos.[25] While searching for the solution, we found a series of important studies of g/u-symmetry breaking or mixing in homonuclear diatomic molecules. The terms in the molecular Hamiltonian that are responsible for rovibronic interactions cannot mix states of different g/u symmetries because they are invariant with respect to all symmetry operations in the $D_{\infty h}$ point group.[26] If the hyperfine Hamiltonian is included, the molecular-symmetry group has to be used, which does not contain the molecular-point-group inversion operation i anymore so that g/u-symmetry mixing can occur. This effect is rather small and only becomes significant when two vibronic states of opposite g/u symmetry become nearly degenerate, as is the case when the dissociation threshold $H^+ + H(1s)$ of H_2^+ is approached and the A^+ and X^+ states become degenerate.

Pique *et al.*[27] reported the first experimental observation of g/u-mixing induced by the hyperfine interaction with the example of molecular iodine.[27–29] The theory of predissociation caused by off-diagonal terms (within the adiabatic approximation) of the hyperfine Hamiltonian, which represents a generalization of type I predissociation, was elaborated by Broyer, Vigué, and Lehmann.[30,31] They calculated the lifetimes of the levels subject to the hyperfine-induced predissociation using Fermi's *golden rule* and evaluated the interaction matrix elements of the Hamiltonian using the wave functions of the bound and continuum states. The treatment of Broyer *et al.*[30,31] cannot be followed in the case of the $H^+ + H(1s)$ collision because this system is dominated, at low energies, by shape resonances. Shape resonances are a *single-channel* effect and one would need to include the coupling to the continuum of another electronic state (a *multi-channel* effect). Fermi's *golden rule* cannot be applied in this case because the perturbation is larger than the energy separation of the unperturbed (continuum) states. The shape resonances of H_2^+ are actually Feshbach resonances when the hyperfine structure is included and can, in principle, be broadened by the hyperfine interaction. Our initial interest in this problem actually arose from a discrepancy between the observed [0.56(8) cm^{-1}] and calculated (0.16 cm^{-1}) widths of the $X^+(17, 7)$ shape resonance of H_2^+,[32] which we initially thought might have its origin in the hyperfine interaction. The reasons for the discrepancy have only been identified very recently.[33]

Moss considered g/u-symmetry breaking in the molecular hydrogen ion[13] in order to explain the spectroscopic observations made by Carrington and co-workers[12] mentioned above. Moss calculated the bound-state level shifts caused by the Fermi-contact hyperfine interaction [see Eq. (22) for the complete hyperfine Hamiltonian of H_2^+] using second-order perturbation theory and assuming an R-independent perturbation term. He found that it was necessary to include the effect of the vibrational continuum in order to reach good agreement with the observed level shifts, which he did by carrying out an explicit, truncated sum over the continuum. He commented in his article that "adding the hyperfine interaction to the adiabatic potentials for the ground and excited electronic states, allowing the Fermi-contact interaction to couple the two potentials and using the new potentials to determine corrected vibration-rotation levels, gave splittings two orders of magnitude too large."[13] This difficulty mentioned by Moss[13] was not encountered in Ref. 20 because only the diagonal terms of the hyperfine Hamiltonian were considered and the hyperfine-interaction-induced g/u mixing was neglected.

We will show in this article for the first time how to rigorously solve the nuclear Schrödinger equation including the hyperfine interaction within the close-coupling approximation, i.e., by considering the coupling of the $X^+ \, ^2\Sigma_g^+$ and $A^+ \, ^2\Sigma_u^+$ states induced by the hyperfine Hamiltonian. The

25 July 2026 18:11:09

treatment is related to the treatment of singlet-triplet mixing in the alkali-metal dimers in Refs. 34 and 35 (see also Ref. 36) and to the treatment of the g/u mixing in H_2 by Pachucki and Komasa.[37] Our results imply that the conclusions reached in earlier work on the existence of the $A^+(1, 0)$ state and on the s-wave scattering length of the $H^+ + H(1s)$ have to be partially revised.

II. COMPUTATIONAL METHODS

In this section, we present an overview of the theoretical and computational methods used in the present work, which include electronic-structure calculations (Subsection II A), nonadiabatic coupled-equations calculations (Subsection II B), and scattering calculations (Subsection II C). Subsection II D shows how these different aspects can be combined to reach a full description of the way the hyperfine interaction affects the structure and dynamics of the $H^+ + H(1s)/H_2^+$ system. An alternative method to treat atomic collisions would involve generalized multichannel quantum-defect theory.[5,38]

In our previous studies of H_2^+,[32,33,39] we considered adiabatic, nonadiabatic, relativistic, and radiative corrections to rovibronic energies, but did not consider the hyperfine interaction. Consequently, the $X^+\ ^2\Sigma_g^+$ and $A^+\ ^2\Sigma_u^+$ states could be treated separately. The nonadiabatic corrections originating from interactions with energetically distant electronic states of Σ and Π symmetries were obtained by using R-dependent vibrational and rotational reduced masses[40,41] and were found to be negligible for all states having wave functions located at large internuclear distances R. In this region, different types of nonadiabatic interactions become important, caused by interactions between the $X^+\ ^2\Sigma_g^+$ and $A^+\ ^2\Sigma_u^+$ states induced by the g/u-mixing Fermi-contact terms of the hyperfine Hamiltonian.[13] The treatment of these latter nonadiabatic interactions is the focus of the present article and requires the consideration of only these two electronic states. Our treatment follows the close-coupling treatment of nonadiabatic interactions of energetically close-lying electronic states used by Dressler and co-workers to study the electronically excited states of H_2.[42]

A. Solution of the electronic Schrödinger equation

The main aspects of the electronic-structure calculations presented in this subsection have been described in Ref. 39 and are repeated here for completeness. The rovibronic (rve) Hamiltonian of the hydrogen molecular ion, expressed in a coordinate system with the origin at the geometric center of the molecule, is given by[43] (R is the separation between the nuclei a and b, $\boldsymbol{r}$ designates the electron coordinates, and cn stands for "clamped nuclei")

$$\mathcal{H}_{\rm rve} = \underbrace{-\frac{\nabla_{\boldsymbol{r}}^2}{2} + \frac{1}{R} - \frac{1}{r_{\rm a}} - \frac{1}{r_{\rm b}}}_{H_{\rm cn}} \underbrace{-\frac{\nabla_{R\Theta\Phi}^2}{2\mu}}_{H_1'} \underbrace{-\frac{\nabla_{\boldsymbol{r}}^2}{8\mu}}_{H_2'}, \tag{1}$$

where $\mu = m_{\rm p}/2$ is the nuclear reduced mass and $r_{\rm a}$ and $r_{\rm b}$ are the distances of the electron to the two nuclei. The electronic Born-Oppenheimer (BO) equation

$$H_{\rm cn}\psi_i(\boldsymbol{r}; R) = U_i^{\rm BO}(R)\psi_i(\boldsymbol{r}; R) \tag{2}$$

is separable in prolate spheroidal coordinates (ξ, η, γ) and can be solved by variational methods.[2,7,44] The explicit expressions for all operators can be obtained from the general two-electron forms derived by Kolos and Wolniewicz[45] by replacing ϕ by 0 and Λ/2 by Λ, as defined in their work. The ansatz for the electronic wave function $\psi_t(\boldsymbol{r}; R)$ used in our calculations is[44]

$$\psi_t(\xi, \eta, \gamma; R) = f(\xi; R)g(\eta; R)n(\gamma), \tag{3}$$

with

$$g(\xi; R) = (\xi^2 - 1)^{\Lambda/2}(\xi + 1)^{(R/p)-\Lambda-1}\exp(-p\xi) \times \sum_{n=0}^{\infty} g_n(R)\left(\frac{\xi - 1}{\xi + 1}\right)^n, \tag{4}$$

$$f(\eta; R) = \sum_{s=0}^{\infty} f_s(R)P_{\Lambda+s}^{\Lambda}(\eta), \text{ and} \tag{5}$$

$$n(\gamma) = \sqrt{\frac{1}{2\pi}}\exp\left[i\Lambda\gamma\right]. \tag{6}$$

$P_{\Lambda+s}^{\Lambda}(\eta)$ are associated Legendre polynomials and $p = R\sqrt{-(U^{\rm BO}(R) - 1/R)/2}$. The expansion coefficients g_n and f_s are determined by requiring that the eigenvalue A simultaneously satisfies

$$\mathbf{G}\cdot\mathbf{g} = -A\mathbf{g} \quad \text{and} \quad \mathbf{F}\cdot\mathbf{f} = A\mathbf{f}, \tag{7}$$

where $\mathbf{G}$ and $\mathbf{F}$ are tridiagonal matrices and are given in terms of R, p, and Λ.[44] In the case of the X^+ and A^+ states of H_2^+, Λ = 0.

B. Calculation of bound rovibronic levels

Because we neglect the rotation-electronic interactions in our treatment of g/u mixing and only consider Σ states (Λ = 0), we have $N = J$ and can expand the rovibronic wave functions $\Xi(\boldsymbol{r}, \boldsymbol{R})$ in a basis of electronic-rotational functions $\psi_i(\boldsymbol{r}; \boldsymbol{R})$,[42]

$$\Xi(\boldsymbol{r}, \boldsymbol{R}) = \frac{1}{R}\sum_i \psi_i(\boldsymbol{r}; \boldsymbol{R})\phi_i(R) = \frac{1}{R}\boldsymbol{\Psi}\cdot\boldsymbol{\phi}, \tag{8}$$

where $\psi_i(\boldsymbol{r}; \boldsymbol{R})$ are products of the electronic functions $\psi_i(\boldsymbol{r}; R)$ and the symmetric-top rotational functions $|N\Lambda M_N\rangle$. $\boldsymbol{R}$ and $\boldsymbol{r}$ represent the internuclear-separation vector and the coordinates of the electron, respectively. Using the ansatz (8) for the total Hamiltonian in Eq. (1), multiplying from the left with $\psi_i(\boldsymbol{r}; \boldsymbol{R})$, and integrating over the rotational and electronic coordinates, one obtains a set of coupled equations[42]

$$\left\{-\frac{1}{2\mu}\left[\mathbf{I}\frac{\mathrm{d}^2}{\mathrm{d}R^2} - \mathbf{I}\frac{N(N+1)}{2R^2} + \boldsymbol{A}(R) + 2\boldsymbol{B}(R)\frac{\mathrm{d}}{\mathrm{d}R}\right] + \boldsymbol{U}(R) - E\right\}\boldsymbol{\phi} = \mathbf{0}, \tag{9}$$

where $\mathbf{I}$ is the identity matrix and $\boldsymbol{U}$ is the diagonal matrix containing the Born-Oppenheimer potential curves

$$U_{ii} = U_i^{\rm BO}(R) = \langle\psi_i|H_{\rm cn}|\psi_i\rangle, \tag{10}$$

25 July 2026 18:11:09

and $\boldsymbol{A}$ and $\boldsymbol{B}$ are the nonadiabatic coupling matrices. For the matrix elements between electronic states having the same value of the orbital-angular-momentum molecule-fixed projection quantum number Λ, one obtains[42]

$$A_{ij}^{\Lambda}(R) = \left\langle \psi_i \left| \frac{\mathrm{d}^2}{\mathrm{d}R^2} - \frac{\boldsymbol{L}^+\boldsymbol{L}^- - \Lambda(\Lambda+1)}{R^2} + \frac{1}{4}\nabla_1^2 \right| \psi_j \right\rangle, \quad (11)$$

$$B_{ij}^{\Lambda}(R) = \left\langle \psi_i \left| \frac{\mathrm{d}}{\mathrm{d}R} \right| \psi_j \right\rangle, \quad (12)$$

where $\boldsymbol{L}^+$ and $\boldsymbol{L}^-$ are the raising and lowering electronic-orbital–angular-momentum operators.[46] The expressions for the off-diagonal block in Λ are not given here, but can be found in Ref. 42.

Because the diagonal elements of $\boldsymbol{B}(R)$ are zero, the adiabatic corrections correspond to the diagonal terms of the nonadiabatic coupling matrix $\boldsymbol{A}(R)$ and are sums of the two integrals[47]

$$\left\langle H_1' \right\rangle_i(R) = \int \psi_i^*(\boldsymbol{r};R) \left[-\frac{\nabla_{R\Theta\Phi}^2}{2\mu} \right] \psi_i(\boldsymbol{r};R)\mathrm{d}\tau, \quad (13)$$

corresponding to the first two terms on the right-hand side of Eq. (11), and

$$\left\langle H_2' \right\rangle_i(R) = \int \psi_i^*(\boldsymbol{r};R) \left[-\frac{\nabla_1^2}{8\mu} \right] \psi_i(\boldsymbol{r};R)\mathrm{d}\tau, \quad (14)$$

corresponding to the third term, using the BO electronic wave functions. The adiabatic potential-energy curves are thus given by $U_i^{\mathrm{ad}}(R) = U_i^{\mathrm{BO}}(R) + \left\langle H_1' \right\rangle_i(R) + \left\langle H_2' \right\rangle_i(R)$.

Bound states of the rovibronic Hamiltonian can be calculated for the system of coupled equations [Eq. (9)] using the renormalized Numerov method introduced in Ref. 48. To take full advantage of the Numerov integration scheme, the dynamical coupling term $2\boldsymbol{B}(R)\frac{\mathrm{d}}{\mathrm{d}R}$ has to be eliminated by a transformation from an adiabatic to a diabatic electronic basis, as introduced in Refs. 42 and 49. This is achieved with the transformation matrix $\boldsymbol{M}$, which satisfies

$$\frac{\mathrm{d}\boldsymbol{M}}{\mathrm{d}R} + \boldsymbol{B}(R)\cdot\boldsymbol{M}(R) = \boldsymbol{0}, \quad (15)$$

where $\boldsymbol{M}$ is an orthogonal matrix, i.e., $\tilde{\boldsymbol{M}}\boldsymbol{M} = \mathbf{I}$. For the calculation of bound rovibronic states, the starting value $\boldsymbol{M}(R_0) = \mathbf{I}$ is usually chosen at small internuclear distances ($R_0 \leq 2$ a$_0$) so that the repulsive part of the diabatic and adiabatic potential-energy curves is identical.

C. Calculation of rovibronic continuum states

In the continuum, we use the scattering-matrix formalism to describe the $H^+ + H(1s)$ system. The scattering matrix $\boldsymbol{S}$ is obtained by applying scattering boundary conditions in the asymptotic region and making sure that the channels are uncoupled for $R \to \infty$.[50] From Eq. (9), we define the effective potential matrix $\boldsymbol{W}(R)$ as

$$\boldsymbol{W}(R) = \boldsymbol{U}(R) - \frac{1}{2\mu}\left[-\mathbf{I}\frac{N(N+1)}{2R^2} + \boldsymbol{A}(R) + 2\boldsymbol{B}(R)\frac{\mathrm{d}}{\mathrm{d}R} \right], \quad (16)$$

which has to be diagonalized in the asymptotic region ($R \to \infty$) using

$$\boldsymbol{W}^{\infty}(R) = \boldsymbol{M}(\infty)\boldsymbol{W}(R)\tilde{\boldsymbol{M}}(\infty) \quad (17)$$

to give

$$W_{ij}^{\infty}(R) \propto \delta_{i,j}\left(U'_i(\infty) + \frac{N(N+1)}{2\mu R^2} \right), \quad (18)$$

where $U'_i(\infty) = k_i^2/(2\mu)$ is the asymptotic channel energy.

Whereas the need for the transformation in Eq. (15) is solely dictated by the numerical integration scheme and therefore optional, the transformation in Eq. (17) is compulsory in order to remove unphysical couplings at infinite distance and to extract meaningful information on the scattering process. The numerically integrated radial wave functions $\boldsymbol{\phi}(\boldsymbol{R})$ are expanded in the Riccati-Bessel functions $j_i(k_iR)$ and $n_i(k_iR)$, which are the solutions for long-range potentials of the form of Eq. (18), leading to

$$\boldsymbol{\phi} = \mathcal{J} + \mathcal{N}\boldsymbol{K}, \quad (19)$$

where $\mathcal{J}$ and $\mathcal{N}$ are diagonal matrices containing the Riccati-Bessel functions j_i and n_i, as explained in Refs. 48 and 51.

At energies E where open and closed channels coexist, the $\boldsymbol{K}$ matrix is expressed in the block form as[52]

$$\boldsymbol{K} = \begin{pmatrix} \boldsymbol{K}_{\mathrm{oo}} & \boldsymbol{K}_{\mathrm{oc}} \\ \boldsymbol{K}_{\mathrm{co}} & \boldsymbol{K}_{\mathrm{cc}} \end{pmatrix}. \quad (20)$$

In the energy range between the $H^+ + H(1s)$ ($F = 0$) and $H^+ + H(1s)$ ($F = 1$) dissociation thresholds, care must be taken to avoid numerical difficulties in the determination of the $\boldsymbol{K}$ matrix because the wave function of the closed $H^+ + H(1s)$ ($F = 1$) channel diverges for $R \to \infty$. We followed the procedure explained in Ref. 52 by replacing the closed-channel elements. This transformation leaves the open-open part $\boldsymbol{K}_{\mathrm{oo}}$ of the $\boldsymbol{K}$ matrix unchanged and the scattering matrix $\boldsymbol{S}$ is obtained by[53]

$$\boldsymbol{S} = (\mathbf{1} + i\boldsymbol{K}_{\mathrm{oo}})^{-1}(\mathbf{1} - i\boldsymbol{K}_{\mathrm{oo}}). \quad (21)$$

D. Hyperfine interaction and g/u-mixing

The effective hyperfine Hamiltonian for the hydrogen molecular ion H_2^+ is given by[54]

$$\begin{aligned} \mathcal{H}_{\mathrm{hfs}} = {} & b_F(\boldsymbol{I}\cdot\boldsymbol{S}) + \gamma_{\mathrm{SR}}(\boldsymbol{N}\cdot\boldsymbol{S}) + c_I(\boldsymbol{N}\cdot\boldsymbol{I}) + \frac{d_1}{(2N-1)(2N+3)} \\ & \times \left(\frac{2}{3}N^2(\boldsymbol{I}\cdot\boldsymbol{S}) - [(\boldsymbol{N}\cdot\boldsymbol{I})(\boldsymbol{N}\cdot\boldsymbol{S}) + (\boldsymbol{N}\cdot\boldsymbol{S})(\boldsymbol{N}\cdot\boldsymbol{I})] \right) \\ & + \frac{d_2}{(2N-1)(2N+3)} \left(\frac{1}{3}N^2I^2 - \frac{1}{2}(\boldsymbol{N}\cdot\boldsymbol{S}) - (\boldsymbol{N}\cdot\boldsymbol{I})^2 \right), \end{aligned} \quad (22)$$

where $\boldsymbol{I}$ is the total nuclear spin and $\boldsymbol{N}$ and $\boldsymbol{S}$ are the rotational and electron-spin angular momenta of H_2^+, respectively. b_F and γ_{SR} are the *Fermi-contact* and the spin-rotation coupling constants, respectively, and have been calculated for the lowest rovibrational levels by Korobov *et al.* at high precision using a pre-Born-Oppenheimer variational ansatz for the wave function.[54] Similar expressions can be derived for D_2^+ and HD^+,[55] which contain additional terms arising from the quadrupole of the deuterons.

25 July 2026 18:11:09

To include the effect of the hyperfine Hamiltonian in the calculations of the spin-rovibronic level energies, we follow the treatment of Moss[13] in the sense that we only consider the Fermi-contact term of the hyperfine interaction [first term on the right-hand side of Eq. (22)] and neglect the spin-rotation interaction and the axial component of the electron-spin–nuclear-spin dipolar interaction. The corresponding terms of the hyperfine Hamiltonian are indeed about two orders of magnitude weaker than the Fermi-contact term.[13,54] In contrast to Moss,[13] however, we implement the hyperfine interaction directly into the rovibronic Hamiltonian [Eq. (9)] as an additional nonadiabatic coupling term $\boldsymbol{A}_{\rm hfs}(R)$. This procedure is, in principle, exact for $N = 0$, the only approximation being the neglect of the weaker terms of the hyperfine Hamiltonian, which affect states with $N \geq 1$.

The two proton spins in H_2^+ couple to give the total nuclear spin $\boldsymbol{I} = \boldsymbol{I_1} + \boldsymbol{I_2}$ [the indices 1 and 2 refer to the protons a and b in Eq. (1)], which is itself coupled to the electron spin $\boldsymbol{S}$ ($S = 1/2$) to give the total spin $\boldsymbol{G} = \boldsymbol{I} + \boldsymbol{S}$. We obtain $G = 1/2$ for $I = 0$ (para) and $G = 1/2$, $3/2$ for $I = 1$ (ortho) H_2^+. Because we neglect the spin-rotation interaction, there are no further splittings for a given rotational level and both G and N become good quantum numbers. By taking into account the restrictions imposed by the Pauli principle for the identical nuclei, we obtain

$$\begin{aligned}
X^{+2}\Sigma_g^+: &\quad \text{even } N \text{ (para)} \Leftrightarrow \text{one component: } G = \frac{1}{2}\\
&\quad \text{odd } N \text{ (ortho)} \Leftrightarrow \text{two components: } G = \frac{1}{2} \text{ and } G = \frac{3}{2},\\
A^{+2}\Sigma_u^+: &\quad \text{even } N \text{ (ortho)} \Leftrightarrow \text{two component: } G = \frac{1}{2} \text{ and } G = \frac{3}{2}\\
&\quad \text{odd } N \text{ (para)} \Leftrightarrow \text{one component: } G = \frac{1}{2}.
\end{aligned}$$

The $G = 3/2$ hyperfine component is thus not affected by g/u-symmetry breaking. For $N = 0$, it has pure $A^+\,{}^2\Sigma_u^+$ character. The two $G = 1/2$ hyperfine components are subject to g/u-symmetry breaking and can be obtained from the effective Hamiltonian

$$\mathcal{H}_{\rm hfs} = b_{\rm F}(i, v/k, N)\boldsymbol{S}\cdot\boldsymbol{I}, \tag{23}$$

where $b_{\rm F}(i, v/k, N)$ is the Fermi-contact parameter for the rovibrational level (v, N) of the electronic state i. In the vibrational continuum, v is replaced by k. The explicit form of the operator of the Fermi-contact interaction is given by[13,30]

$$\mathcal{H}_{\rm FC} = \underbrace{\frac{8\pi}{3}\frac{g g_{\rm p}\mu_{\rm B}\mu_{\rm N}}{4\pi\epsilon_0 c^2}}_{K}[\boldsymbol{S}\cdot\boldsymbol{I}_1\delta(\boldsymbol{r}-\boldsymbol{R}_{\rm a}) + \boldsymbol{S}\cdot\boldsymbol{I}_2\delta(\boldsymbol{r}-\boldsymbol{R}_{\rm b})], \tag{24}$$

where $\boldsymbol{r}$ is the electron coordinate with respect to the geometric center, g and $g_{\rm p}$ are the electron g-factor and proton gyromagnetic ratio, respectively, and $\mu_{\rm B}$ and $\mu_{\rm N}$ the Bohr magneton and the nuclear magneton, respectively. The proportionality constant K can be expressed in atomic units using

$$\mu_{\rm B} = \frac{e\hbar}{2m_{\rm e}} \quad \Leftrightarrow \quad \frac{1}{2}\ \text{a.u.}, \tag{25}$$

$$\mu_{\rm N} = \frac{m_{\rm e}}{m_{\rm p}}\mu_{\rm B} \quad \Leftrightarrow \quad \frac{1}{2m_{\rm p}}\ \text{a.u.} \tag{26}$$

as

$$K = \frac{8\pi}{3}\frac{g g_{\rm p}\alpha^2}{4m_{\rm p}}, \tag{27}$$

with $g = 2.002\,319\,304\,361\,82$ and $g_{\rm p} = 5.585\,694\,702$.[56]

In the limiting case of the hydrogen atom, i.e., for the dissociated H_2^+ ion with charge localization, we obtain from Eq. (24) using $\langle\delta(\boldsymbol{r})\rangle = 1/\pi$[57]

$$\begin{aligned}
\langle\mathcal{H}_{\rm FC}\rangle &= K\langle\boldsymbol{S}\cdot\boldsymbol{I}_1\rangle\langle\delta(\boldsymbol{r})\rangle = \frac{K}{2}\left\langle\boldsymbol{F}^2 - \boldsymbol{S}^2 - \boldsymbol{I}_1^2\right\rangle\langle\delta(\boldsymbol{r})\rangle\\
&= \frac{K}{2}(F(F+1) - S(S+1) - I_1(I_1+1))\langle\delta(\boldsymbol{r})\rangle\\
&= \frac{K}{2\pi}(F(F+1) - \frac{3}{2}) = \begin{cases} -\frac{3K}{4\pi} & \text{for } F = 0,\\ +\frac{K}{4\pi} & \text{for } F = 1. \end{cases}
\end{aligned} \tag{28}$$

Neglecting the dipolar interaction, the hyperfine splitting in the 1s state of the hydrogen atom is thus $\Delta E_{\rm hfs}/h = (K/\pi)(E_{\rm h}/h) \approx 1422.807\,58$ MHz (see Ref. 57 for a complete discussion).

Figure 1 illustrates the correlation between the hyperfine structures of the H_2^+ ion at short internuclear distances and the $H^+ + H(1s, F)$ collision at $R \to \infty$. The total spin $\boldsymbol{G} = \boldsymbol{I}_1 + \boldsymbol{I}_2 + \boldsymbol{S}$ is conserved for $N = 0$ and also for other N values if the spin-rotation interactions are neglected. I and F

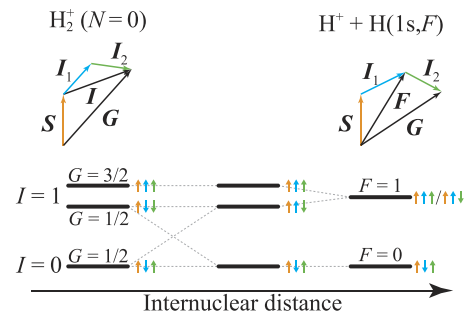


FIG. 1. Correlation diagram connecting the short range (H_2^+) and long range [$H^+ + H(1s, F)$] spin-angular-momentum coupling cases. The colored arrows give the relative orientation of the electron and nuclear spins.

25 July 2026 18:11:09

are good quantum numbers at short and large internuclear distances, respectively. The colored arrows indicate schematically the relative orientation of the electron and proton spins.

To obtain the matrix elements of $\mathcal{H}_{\rm FC}$ in Eq. (24), the ansatz

$$|\Psi\rangle = \sum_{g,u} |\Sigma_{\rm g/u}; v; N\rangle |N\Lambda M_N\rangle |S(I_1I_2)IG\rangle \tag{29}$$

for the molecular wave function is used, where $|\Sigma_{\rm g/u}; v; N\rangle$ is the vibronic wave function with vibrational quantum number v (in the continuum, v is replaced by k; see above) in the effective potential with rotational quantum number N. $\Sigma_{\rm g/u}$ designates the $X^+\,^2\Sigma_g^+$ or the $A^+\,^2\Sigma_u^+$ electronic state so that $\Lambda = 0$. $|N\Lambda M_N\rangle$ stands for the rotational wave function that is uncoupled from the spin wave function $|S(I_1I_2)IG\rangle$, as discussed above.

None of the operators in Eq. (24) act on the rotational wave functions because the spin-rotation coupling is neglected. Consequently, we obtain

$$\begin{aligned}
&\left\langle \Sigma'_{\rm g/u}\middle|\left\langle N'\Lambda'M'_N|\langle S(I_1I_2)I'G'|\mathcal{H}_{\rm FC}|S(I_1I_2)IG\rangle|N\Lambda M_N\right\rangle|\Sigma_{\rm g/u}\right\rangle \\
&\quad = \delta_{N',N}\delta_{\Lambda',\Lambda}\delta_{M'_N,M_N}\left\langle \Sigma'_{\rm g/u}|\langle S(I_1I_2)I'G'|\mathcal{H}_{\rm FC}|\right. \\
&\qquad \left. S(I_1I_2)IG\rangle|\Sigma_{\rm g/u}\right\rangle \\
&\quad = K\Big[\left\langle \Sigma_{\rm g/u}{}'|\delta(\boldsymbol{r}-\boldsymbol{R}_{\rm a})|\Sigma_{\rm g/u}\right\rangle\langle S(I_1I_2)I'G'|\boldsymbol{S}\cdot\boldsymbol{I}_1|S(I_1I_2)IG\rangle \\
&\qquad + \left\langle \Sigma'_{\rm g/u}|\delta(\boldsymbol{r}-\boldsymbol{R}_{\rm b})|\Sigma_{\rm g/u}\right\rangle\langle S(I_1I_2)I'G'|\boldsymbol{S}\cdot\boldsymbol{I}_2|S(I_1I_2)IG\rangle\Big],
\end{aligned} \tag{30}$$

which implies conservation of the rotational-angular momentum $\boldsymbol{N}$ and of its projections $\hbar\Lambda$ and $\hbar M$ along the molecular axis and the space-fixed axis, respectively, as expected. Note that the integration over the vibrational coordinate R is carried out when solving the system of coupled equations [see Eq. (9)].

Next, we consider the expectation value of the delta functions in the Fermi-contact terms, which is responsible for the g/u-symmetry breaking. For symmetry reasons, we find

$$\underbrace{\langle\Sigma_{\rm g}|}_{+}\,\delta(\boldsymbol{r}-\boldsymbol{R}_{\rm a})\,\underbrace{|\Sigma_{\rm g}\rangle}_{+} = \underbrace{\langle\Sigma_{\rm g}|}_{+}\,\delta(\boldsymbol{r}-\boldsymbol{R}_{\rm b})\,\underbrace{|\Sigma_{\rm g}\rangle}_{+}, \tag{31}$$

$$\underbrace{\langle\Sigma_{\rm u}|}_{+}\,\delta(\boldsymbol{r}-\boldsymbol{R}_{\rm a})\,\underbrace{|\Sigma_{\rm u}\rangle}_{+} = \underbrace{\langle\Sigma_{\rm u}|}_{-}\,\delta(\boldsymbol{r}-\boldsymbol{R}_{\rm b})\,\underbrace{|\Sigma_{\rm u}\rangle}_{-} \tag{32}$$

and

$$\underbrace{\langle\Sigma_{\rm g}|}_{+}\,\delta(\boldsymbol{r}-\boldsymbol{R}_{\rm a})\,\underbrace{|\Sigma_{\rm u}\rangle}_{+} = -\underbrace{\langle\Sigma_{\rm g}|}_{+}\,\delta(\boldsymbol{r}-\boldsymbol{R}_{\rm b})\,\underbrace{|\Sigma_{\rm u}\rangle}_{-}, \tag{33}$$

$$\underbrace{\langle\Sigma_{\rm u}|}_{+}\,\delta(\boldsymbol{r}-\boldsymbol{R}_{\rm a})\,\underbrace{|\Sigma_{\rm g}\rangle}_{+} = -\underbrace{\langle\Sigma_{\rm u}|}_{-}\,\delta(\boldsymbol{r}-\boldsymbol{R}_{\rm b})\,\underbrace{|\Sigma_{\rm g}\rangle}_{+}. \tag{34}$$

The signs indicated below the bras and kets represent the signs of the electronic wave functions at the position of the nucleus upon which the delta function acts and correspond to the sign convention for the electronic wave functions given in Fig. 2. The electron density $\rho_{\rm g/u}$ at the positions of the nuclei

$$\rho_{\rm g/u}(R_j) = \langle\Sigma_{\rm g/u}|\delta(\boldsymbol{r}-\boldsymbol{R}_j)|\Sigma_{\rm g/u}\rangle = |\Sigma_{\rm g/u}(R_j)|^2, \quad \text{where } j = a, b, \tag{35}$$

is a function of the internuclear distance R, and so are the diagonal and off-diagonal matrix elements in Eq. (30), for which we obtain

$$\begin{aligned}
\langle\mathcal{H}_{\rm FC}\rangle_{\rm diag} = K\rho_{\rm g/u}\Big[&\langle S(I_1I_2)I'G'|\boldsymbol{S}\cdot\boldsymbol{I}_1|S(I_1I_2)IG\rangle \\
&+\langle S(I_1I_2)I'G'|\boldsymbol{S}\cdot\boldsymbol{I}_2|S(I_1I_2)IG\rangle\Big]
\end{aligned} \tag{36}$$

and

$$\begin{aligned}
\langle\mathcal{H}_{\rm FC}\rangle_{\rm off\text{-}diag} = K\left(\rho_{\rm g}\rho_{\rm u}\right)^{\frac{1}{2}}\Big[&\langle S(I_1I_2)I'G'|\boldsymbol{S}\cdot\boldsymbol{I}_1|S(I_1I_2)IG\rangle \\
&-\langle S(I_1I_2)I'G'|\boldsymbol{S}\cdot\boldsymbol{I}_2|S(I_1I_2)IG\rangle\Big],
\end{aligned} \tag{37}$$

respectively.

The matrix elements of the operator $\boldsymbol{S}\cdot\boldsymbol{I}_j$ in the *equal-coupling* representation[58,59] (i.e., the two nuclear spins $I_1 = I_2$ of a homonuclear molecule are first coupled together) can be obtained using standard angular-momentum algebra[46] and are given by

$$\begin{aligned}
\langle\ldots|\boldsymbol{S}\cdot\boldsymbol{I}_1|\ldots\rangle \pm \langle\ldots|\boldsymbol{S}\cdot\boldsymbol{I}_2|\ldots\rangle \propto\ & \delta_{G',G}(-1)^{S+2I_1+I'+G+1} \\
&\times\sqrt{(2I+1)(2I'+1)}\sqrt{S(S+1)(2S+1)} \\
&\times\sqrt{I_1(I_1+1)(2I_1+1)} \\
&\times\begin{Bmatrix} G & I' & S \\ 1 & S & I \end{Bmatrix}\begin{Bmatrix} I_1 & I' & I_1 \\ I & I_1 & 1 \end{Bmatrix} \\
&\times\left((-1)^I \pm (-1)^{I'}\right),
\end{aligned} \tag{38}$$

where the terms in curly brackets are 6j symbols.[46]

The total spin angular momentum $\boldsymbol{G}$ is conserved so that the $G = 3/2$ components in the case of H_2^+ are not affected by the g/u interaction, because for an even (odd) value of N, the $G = 3/2$ levels in the X^+ (A^+) state are forbidden by the Pauli principle and $\boldsymbol{N}$ is also conserved [see Eq. (30)]. The off-diagonal, g/u-symmetry-breaking terms are nonzero only if

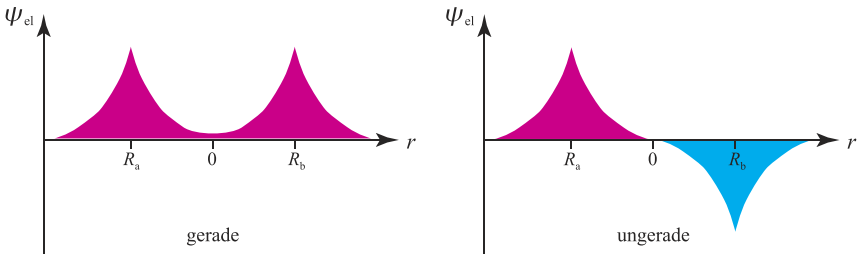


FIG. 2. Schematic illustration of a gerade (left) and ungerade (right) electronic wave function along the internuclear axis.

25 July 2026 18:11:09

$$\Delta I = I - I' = \pm 1, \pm 3, \ldots, \tag{39}$$

which implies that the g/u-symmetry breaking is at the same time also an *ortho-para* symmetry breaking, corresponding to a reorientation of one nuclear spin with respect to the other.

From the expression on the right-hand side of Eq. (38), we obtain the matrix elements

$$\begin{array}{c} |\Sigma_{g/u} IG\rangle\ |\Sigma_g 0\tfrac{1}{2}\rangle\ |\Sigma_u 1\tfrac{1}{2}\rangle \\ \langle\Sigma_g 0\tfrac{1}{2}| \\ \langle\Sigma_u 1\tfrac{1}{2}| \end{array} \begin{pmatrix} 0 & \frac{\sqrt{3}}{2} \\ \frac{\sqrt{3}}{2} & -1 \end{pmatrix} \tag{40}$$

for even N values and

$$\begin{array}{c} |\Sigma_{g/u} IG\rangle\ |\Sigma_g 1\tfrac{1}{2}\rangle\ |\Sigma_u 0\tfrac{1}{2}\rangle \\ \langle\Sigma_g 1\tfrac{1}{2}| \\ \langle\Sigma_u 0\tfrac{1}{2}| \end{array} \begin{pmatrix} -1 & \frac{\sqrt{3}}{2} \\ \frac{\sqrt{3}}{2} & 0 \end{pmatrix} \tag{41}$$

for odd N values.

In the close-coupling approximation that takes into account only the $X^+\ ^2\Sigma_g^+$ and $A^+\ ^2\Sigma_u^+$ states and by combining Eqs. (36), (37), (40), and (41), we find the hyperfine-induced g/u-mixing nonadiabatic coupling matrix $\boldsymbol{A}_{\rm hfs}(R)$ [see Eq. (9)] to be

$$\boldsymbol{A}_{\rm hfs}(R) = \begin{pmatrix} 0 & \frac{\sqrt{3}}{2} K \left(\rho_g(R)\rho_u(R)\right)^{\frac{1}{2}} \\ \frac{\sqrt{3}}{2} K \left(\rho_g(R)\rho_u(R)\right)^{\frac{1}{2}} & -K\rho_u(R) \end{pmatrix} \quad \text{for even } N \text{ values} \tag{42}$$

and

$$\boldsymbol{A}_{\rm hfs}(R) = \begin{pmatrix} -K\rho_g(R) & \frac{\sqrt{3}}{2} K \left(\rho_g(R)\rho_u(R)\right)^{\frac{1}{2}} \\ \frac{\sqrt{3}}{2} K \left(\rho_g(R)\rho_u(R)\right)^{\frac{1}{2}} & 0 \end{pmatrix} \quad \text{for odd } N \text{ values.} \tag{43}$$

The diagonal (blue for X^+ and magenta for A^+) and off-diagonal (green) terms of $\boldsymbol{A}_{\rm hfs}(R)$ are displayed as a function of the internuclear distance in Fig. 3. The off-diagonal term does not vanish for $R \to \infty$ and is needed to obtain the correct dissociation products $H^+ + H(1s)$ ($F = 0$) and $H^+ + H(1s)$ ($F = 1$).

The hyperfine interaction does not give rise to a dynamic nonadiabatic coupling, i.e., $\boldsymbol{B}_{\rm hfs}(R) = 0$ in Eq. (9). Because we neglect rovibronic couplings (see below), we only retain the diagonal (adiabatic) elements of $\boldsymbol{A}(R)$ [see Eq. (11)], to which we add $\boldsymbol{A}_{\rm hfs}(R)$ from Eqs. (42) and (43). This procedure implies that we can replace J (the total-angular-momentum quantum number without nuclear spin) by N (the rotational angular momentum quantum number in Σ electronic states) and $\boldsymbol{U}(R)$ by $\boldsymbol{U}^{\rm ad}(R)$ in Eq. (9) so that the effective potential matrix is

$$\boldsymbol{W}(R) = \left[\boldsymbol{U}^{\rm ad}(R) + \mathbf{I}\frac{N(N+1)}{2\mu R^2} + \boldsymbol{A}_{\rm hfs}(R)\right]. \tag{44}$$

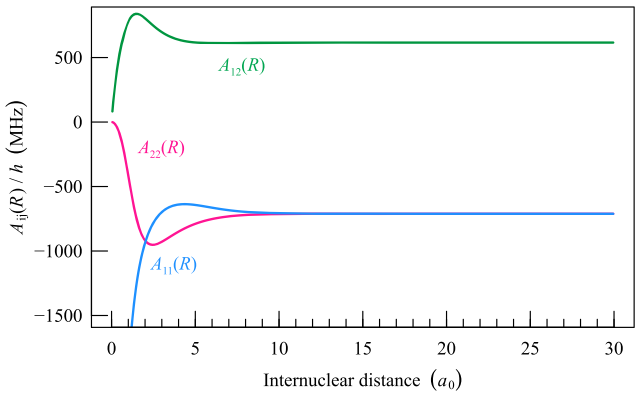


FIG. 3. Nonadiabatic g/u coupling elements in H_2^+ arising from the hyperfine interaction $\boldsymbol{A}_{\rm hfs}(R)$ as a function of the internuclear distance. The subscript "hfs" has been omitted for clarity.

In close-coupling scattering calculations of the X^+ and A^+ states including the hyperfine interaction, the transformed potential $\boldsymbol{W}^\infty(R)$ is uncoupled asymptotically [see Eqs. (17) and (18)].

As an illustration, the effective potentials $\boldsymbol{U}^{\rm ad}(R)$, $\boldsymbol{W}(R)$, and $\boldsymbol{W}^\infty(R)$ [see Eqs. (44) and (17)] of the X^+ and A^+ states for $G = 1/2$ coupled by the hyperfine interaction are displayed in Figs. 4 and 5 for $N = 0$ [which will be used below in the discussion of the behavior of even-N states and of the existence of the $G = 1/2$ hyperfine component of the $A^+(1, 0)$ state] and for $N = 7$ (which is representative of the behavior of odd-N states), respectively. In each of these figures, the thick gray lines correspond to the adiabatic potential-energy functions calculated as explained in Subsections II A and II B. The upper and lower panels depict the diagonal terms (W_{11} and W_{11}^∞ as dashed and solid blue lines and W_{22} and W_{22}^∞ as dashed and solid magenta lines) and off-diagonal terms (W_{12} and W_{12}^∞ as dashed and solid green lines) of the potential matrices, respectively. The regions of short and large internuclear distances are presented in the left and right panels, respectively.

By construction, the off-diagonal coupling elements of $\boldsymbol{W}^\infty(R)$ vanish asymptotically so that, at large R values, the diagonal elements W_{11}^∞ and W_{22}^∞ are separated by the hyperfine splitting of the hydrogen atom (see the discussion above).

25 July 2026 18:11:09

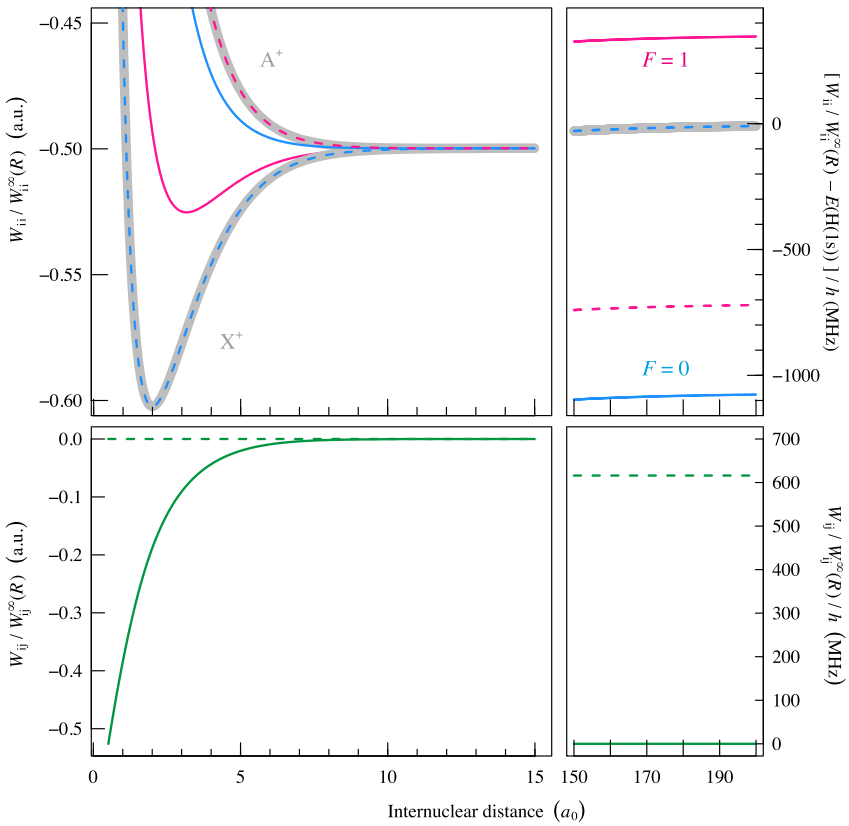


FIG. 4. Effective potentials $\boldsymbol{W}(R)$ and $\boldsymbol{W}^{\infty}(R)$ at small (left) and large (right) internuclear distances: diagonal (upper panel) and off-diagonal (lower panel) elements for $N = 0$. Upper panel: W_{11} (dashed blue); W_{22} (dashed magenta); W_{11}^{∞} (solid blue); W_{22}^{∞} (solid magenta). Lower panel: W_{12} (dashed green); W_{12}^{∞} (solid green). The adiabatic potential energy curves U^{ad} for the X^+ and A^+ state are shown as gray lines in the upper panel.

By contrast, the spacing between W_{11} and W_{22} is less than the splitting between the $F = 0$ and $F = 1$ H(1s) hyperfine components because W_{12} is nonzero. The correct hyperfine splitting at $R = \infty$ is obtained by diagonalizing the matrix $\boldsymbol{W}(R = \infty)$. At short internuclear distances, W_{11} and W_{22} cannot be distinguished from the adiabatic potential functions of the X^+ and A^+ states on the scale of the figure because the elements of $\boldsymbol{A}_{\mathrm{hfs}}(R)$ are all much smaller than the adiabatic

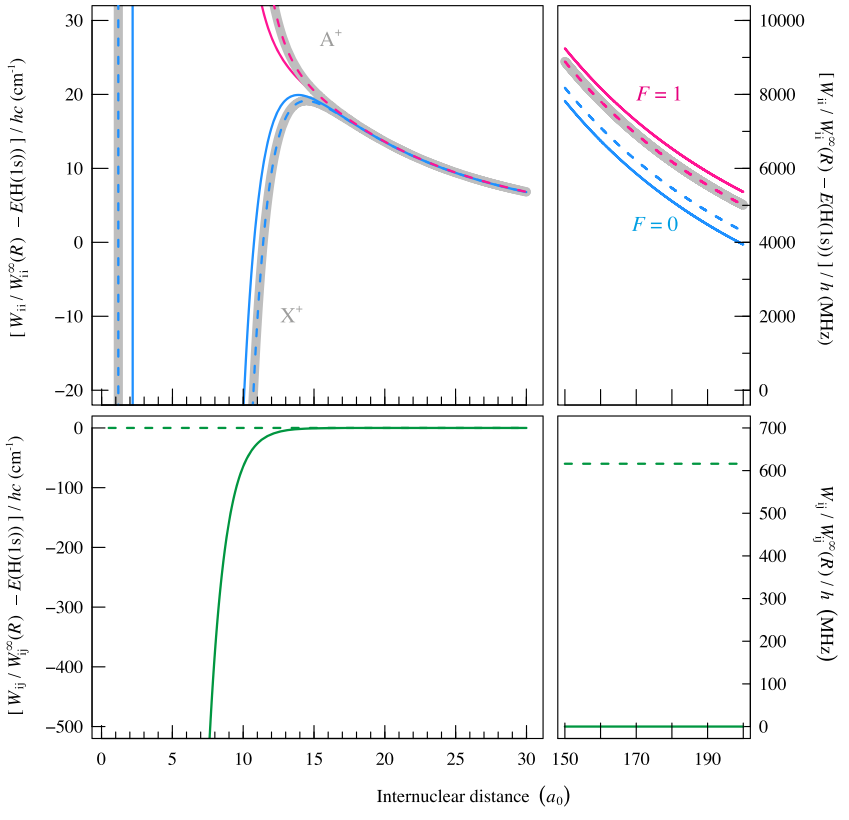


FIG. 5. Effective potentials $\boldsymbol{W}(R)$ and $\boldsymbol{W}^{\infty}(R)$ at small (left) and large (right) internuclear distances: diagonal (upper panel) and off-diagonal (lower panel) elements for $N = 7$. Upper panel: W_{11} (dashed blue); W_{22} (dashed magenta); W_{11}^{∞} (solid blue); W_{22}^{∞} (solid magenta). Lower panel: W_{12} (dashed green); W_{12}^{∞} (solid green). The adiabatic potential energy functions U^{ad} for the X^+ and A^+ state are shown as gray lines in the upper panel.

25 July 2026 18:11:09

electronic energies and their difference. At large internuclear distances, W_{11} exactly coincides with the adiabatic potential functions for even N values, whereas for odd N, it is W_{22} which coincides with these functions. The asymptotic behavior also reveals that, for even N values, W_{11}^{∞} and W_{22}^{∞} correlate to the upper ($F = 1$) and lower ($F = 0$) hyperfine components of the H(1s) dissociation product, respectively, whereas the opposite is true for odd N values. At short range, W_{11}^{∞} and W_{22}^{∞} strongly deviate from the adiabatic potential functions of the X^+ and A^+ states and W_{12}^{∞} becomes large and negative.

When determining the scattering $\boldsymbol{K}$ and $\boldsymbol{S}$ matrices on the basis of Eqs. (17)–(21) by matching to the Riccati-Bessel functions, it is important that $\boldsymbol{M}$ is *independent* of R. Otherwise, the transformation would introduce radial couplings that would give rise to nonzero elements in the $\boldsymbol{B}$ matrix [see Eq. (15)].

III. RESULTS

Exact nonadiabatic energies can, in principle, be determined by solving the system of coupled equations (9), in which $\boldsymbol{A}_{\rm hfs}(R)$ is added to $\boldsymbol{A}(R)$. An infinite number of coupled bound and continuum electronic states must be considered to obtain exact numerical results, which is not possible in practice. Approximate treatments of the nonadiabatic interactions with distant electronic states typically rely on the introduction of R-dependent reduced masses for the vibrational and rotational nuclear motion.[60,61]

In our previous investigations of the weakly bound and quasi-bound levels of the X^+ and A^+ states of H_2^+, we have verified that vibronic nonadiabatic corrections originating from the interaction with distant states do not exceed 1% of the binding energy.[32,39] Moreover, Carbonell *et al.*[19,20] have shown that nonrelativistic and quantum-electrodynamics corrections make a contribution of less than 0.3% to the binding energy of the $A^+(v = 1, N = 0)$ level. We therefore neglect vibronic nonadiabatic, relativistic, and quantum-electrodynamics corrections in our calculations, but include the g/u-symmetry-breaking hyperfine interaction in close-coupling nonadiabatic calculations of the X^+ and A^+ states for $G = 1/2$. In the calculations, we used the procedure outlined in Sec. II. Further details specific to our calculation procedure can be found in Refs. 32 and 39.

We first present the results we obtained for the weakly bound high-vibrational levels of the X^+ state in Subsection III A, then proceed, in Subsection III B, to analyze the effects of the hyperfine interaction on the shape resonances of H_2^+ observed in Refs. 32, and finally discuss the implications of the hyperfine interaction on the existence of the $A^+(v^+ = 1, N^+ = 0)$ state in Subsection III C and on the $H^+ + H(1s)$ scattering length in Subsection III D.

A. Hyperfine-induced g/u-mixing and line shifts

In this section, we present our results concerning the hyperfine-induced g/u-symmetry breaking and its effects on the weakly bound states associated with the X^+ state of H_2^+. To validate our treatment of the g/u interaction, we calculated the expected shifts for different rovibrational levels of the X^+ state and compared our results to the values obtained by Moss[13] in a perturbative treatment, as described in the Introduction.

Our calculations are based on Eq. (44) and on the adiabatic potential curves of the X^+ and A^+ states obtained as explained in Subsections II A and II B. The nonadiabatic coupling between the X^+ and A^+ states originates from the off-diagonal elements of the hyperfine interaction matrix $\boldsymbol{A}_{\rm hfs}(R)$. The hyperfine-induced level shifts of the highest bound levels of the X^+ state were determined by solving the systems of coupled equations and are presented in Table I, where they are compared with the results of Moss.[13]

The level shifts we calculate agree within 10 kHz with the results reported by Moss, except for the $X^+(18, 2)$, (19, 0), and (19, 1) levels. The largest discrepancies between our results and those of Moss do not exceed 300 kHz and might be attributed to the simplified treatment of the continuum and the use of R-independent coupling parameters in Ref. 13, and we conclude that our procedure adequately takes into account the g/u-mixing effects of the hyperfine interaction. Bound states can also be calculated using the transformed potential matrix $\boldsymbol{W}^{\infty}(R)$, and we have verified that the level energies do not depend on whether the effective potential is transformed or not, as expected.

The calculations of Moss presented in Table I show that the contribution of the continuum to the g/u-symmetry-breaking correction becomes the dominant part for the highest rovibrational levels. One would therefore expect an effect of the hyperfine interaction on the position and widths of the shape resonances of H_2^+.

B. Contribution of the hyperfine-induced predissociation to the lifetimes of the $X^+(17, 7)$ and (18, 4) shape resonances

In our previous study of the shape resonances of H_2, we have observed the $X^+(17, 7)$ and (18, 4) resonances and compared their positions and widths to the positions and widths calculated without considering the hyperfine interaction. Whereas we found agreement between calculations and experiment for the positions of both resonances and for the width of the $X^+(18, 4)$, the calculated width of the $X^+(17, 7)$ resonance was found to be about four times narrower than observed. Because the $X^+(17, 7)$ has nominal ortho ($I = 1$) character, we first

TABLE I. Electronic g/u-symmetry-breaking corrections (in MHz) to the dissociation energies of the highest vibrational levels of the ground electronic state of H_2^+ with $G = 1/2$.

	Moss[13]			
Level	Bound contribution	Continuum contribution	Total	This work
(18, 0)	+0.211	+0.152	+0.36	+0.365
(18, 1)	+0.243	+0.174	+0.42	+0.419
(18, 2)	+0.317	+0.526	+0.84	+0.574
(18, 3)	···	+1.031	+1.03	+1.040
(19, 0)	−2.101	+4.879	+2.78	+2.838
(19, 1)	−2.035	+11.911	+9.88	+10.170

25 July 2026 18:11:09

thought that the cause of the discrepancy might be related to the hyperfine interaction.

For the shape resonances (strictly speaking, they should be considered as Feshbach resonances when the hyperfine interaction is considered), the coupled equations were solved up to $R > 200$ a_0 using the transformed potential $\boldsymbol{W}^{\infty}(R)$. To determine the resonance positions and widths, the $\boldsymbol{K}$ matrix was extracted following the procedure described in Subsection II C. The eigenphases $\tilde{\eta}_\alpha$ and $\tilde{\eta}_\beta$ and their energy dependences were determined from the $\boldsymbol{S}$ matrix [Eq. (21)] using

$$\tilde{\boldsymbol{S}} = \boldsymbol{P}^{-1}\boldsymbol{S}\boldsymbol{P} = \begin{pmatrix} e^{2i\tilde{\eta}_\alpha} & 0 \\ 0 & e^{2i\tilde{\eta}_\beta} \end{pmatrix}, \tag{45}$$

and the eigenphase sum was monitored as a function of the energy.[62] In Eq. (45), $\tilde{\eta}_\alpha$ ($\tilde{\eta}_\beta$) corresponds to $\tilde{\eta}_{A^+}$ ($\tilde{\eta}_{X^+}$) and $\tilde{\eta}_{X^+}$ ($\tilde{\eta}_{A^+}$) in the case of even and odd N values, respectively (see Figs. 4 and 5), for collision energies significantly larger than the hyperfine splitting in the hydrogen atom (see Fig. 8 below and related discussion). The resonance positions and widths were then extracted from the eigenphases as explained in Ref. 39.

Table II summarizes the results obtained for the $X^+(17, 7)$ and $X^+(18, 4)$ resonances that were observed in Ref. 32. In order to assess the role of the hyperfine interaction, the calculations were performed for the adiabatic potentials with and without the g/u-symmetry-breaking coupling terms.

Nonadiabatic effects could, in principle, be included in the coupled-equation approach by explicitly taking into account the coupling to the higher $^2\Sigma^+$ and $^2\Pi$ states of H_2^+ in Eq. (9). However, we showed in Ref. 39 that the inclusion of the nonadiabatic interactions did not change the calculated line widths for the $X^+(17, 7)$ and (18, 4) shape resonances by more than 0.02 cm^{-1}, which is much smaller than, and cannot be the explanation for, the observed broadening of 0.56(8) cm^{-1} for the $X^+(17, 7)$ resonance. Table II indicates that the corrections to the positions of the resonances caused by the hyperfine interaction are larger than those for the bound states. Neither the broadening of the $G = 1/2$ component nor the splitting of about 1 GHz between the $G = 1/2$ and 3/2 components is, however, large enough to explain the experimental results for the $X^+(17, 7)$ resonance, which thus must have another origin. We refer to Ref. 33 for the interpretation of this effect.

C. The $A^+(1, 0)$ state of H_2^+

In this section, the influence of the g/u-symmetry breaking on the existence of the presumed $A^+(1, 0)$ state[19,20] is studied. This state is thought to be responsible for the large proton–hydrogen-atom scattering length. The long-range behavior of the proton–hydrogen-atom molecular potential is governed by the charge–induced-dipole interaction that is proportional to $-1/R^4$. The proportionality constant is half the polarizability of the hydrogen atom, i.e., $\alpha/2 = 9/4$ in atomic units.[63] The charge–induced-dipole interaction is attractive. As R decreases, the electron-exchange forces, which are attractive for the electronic ground state and repulsive for the first excited electronic state of H_2^+, become dominant. The A^+ potential is therefore mainly repulsive and supports only the (0,0), (0,1), and (0,2) states and potentially also the (1,0) state.

The adiabatic potential of the A^+ state, calculated within the single A^+ channel and thus neglecting the hyperfine-induced g/u-symmetry breaking, is depicted in Fig. 6. This potential is adequate to describe states with total spin quantum number $G = 3/2$ that are not subject to the g/u-symmetry-breaking part of the hyperfine interaction. The binding energies of the $G = 3/2$ states one obtains are given with respect to the $H^+ + H(1s, F = 1)$ upper dissociation threshold. The calculated adiabatic dissociation energy of the $A^+(1, 0)$ state we determine with this potential is 7.0067 MHz, and its wave function, also depicted in Fig. 6, has a considerable amplitude up to 5000 a_0. The nonrelativistic dissociation energy of this state was determined to be 7.139 254 798(7) MHz in Ref. 19 and the energy including relativistic and radiative corrections is 7.120 664(3) MHz,[20] both results differing from our approximate result by less than 150 kHz. Consequently, the nonadiabatic, relativistic, and radiative corrections do not significantly modify the properties of this state, as expected.

The coupled equations [Eq. (9)] including the hyperfine-induced g/u-symmetry breaking were solved up to $R_{max} = 20\,000$ a_0. We first varied the strength of the hyperfine-induced g/u-symmetry-breaking interaction $\mathcal{H}_{FC}$ [see Eq. (24)]

TABLE II. Electronic g/u-symmetry-breaking corrections to the widths and dissociation energies of the $X^+(17, 7)$ and (18, 4) shape resonances of H_2^+ with $G = 1/2$ calculated in the adiabatic (AD) approximation. The dissociation energies are taken from Ref. 32.

	AD		AD + g/u mixing		g/u correction	
Level	E_{res}/h (cm^{-1})	Γ (cm^{-1})	E_{res}/h (cm^{-1})	Γ (cm^{-1})	$\Delta E_{res}/h$ (MHz)	$\Delta\Gamma$ (MHz)
(17, 7)	−11.2101	0.1765	−11.1875	0.1796	678	92
(18, 4)	−1.8794	0.2048	−1.8775	0.2019	57.64	−87

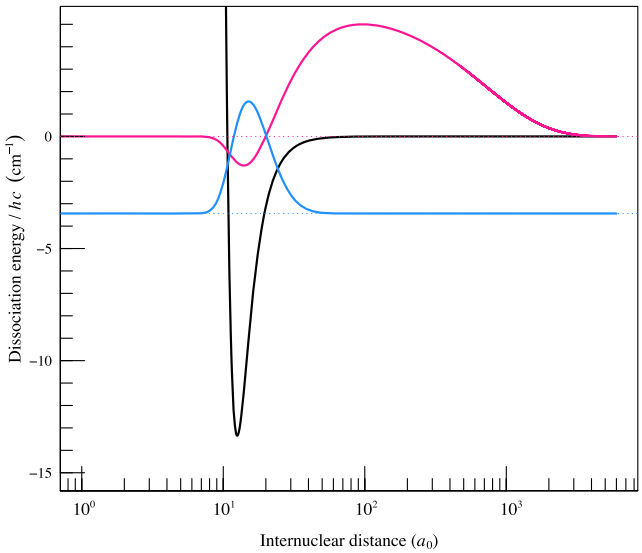


FIG. 6. Adiabatic potential of the A^+ state (black) of the molecular hydrogen ion. The vibrational wave functions of the A^+ (0,0) and (1,0) states of H_2^+ calculated without consideration of the hyperfine interaction are displayed in blue and magenta, respectively, and the corresponding dissociation energies are indicated by dotted lines of the corresponding color.

25 July 2026 18:11:09

by varying a scaled hyperfine-coupling constant K_{scaled} to (i) validate our implementation of the numerical integration of the coupled-equations by reproducing the single-channel dissociation energy for $\boldsymbol{A}_{\text{hfs}}(R) = \mathbf{0}$ and (ii) observe the gradual change of the $A^+(1, 0)$ dissociation energy while increasing K_{scaled} from 0 to its final value K given by Eq. (27).

The calculated dissociation energies of the $A^+(1, 0)$ level with respect to the $H^+ + H(1s)$ ($F = 0$) dissociation threshold are depicted as a function of K_{scaled} in Fig. 7. In the coupled-equation calculations, which no longer distinguish between X^+ and A^+ states, the $A^+(1, 0)$ state appeared as the 22nd state with $N^+ = 0$ because there are 20 vibrational states related to the X^+ potential and the $A^+(0, 0)$ at lower energies. Figure 7 indicates that the dissociation energy of the $A^+(1, 0)$ state gradually decreases when the hyperfine coupling constant K_{scaled} is increased from zero to its actual value of $K \approx 4469.88$ MHz. For a g/u coupling strength exceeding 14% of K in Eq. (27), the level is shifted above the $H^+ + H(1s)$ ($F = 0$) dissociation limit.

Because the $A^+(1, 0)$ state with $G = 1/2$ has the character of the $H^+ + H(1s)$ ($F = 0$) dissociation channel, there is no possibility that this state could emerge as a $F = 1$ Feshbach resonance between the $H^+ + H(1s)$ ($F = 0$) and $H^+ + H(1s)$ ($F = 1$) dissociation limits. We therefore conclude that this state does not exist, which has implications on the sign and magnitude of the scattering length of the $H^+ + H(1s)$ collision. This conclusion is supported by the fact that the calculated phase does not exhibit any jump of π between the two dissociation limits.

D. Scattering length of the $H^+ + H(1s)$ collision

Given that the $A^+(1, 0)$ state was identified as the reason for the large positive value [750(5) a_0] of the scattering length of the $H^+ + H(1s)$ collision reported in Refs. 19 and 20, we made a new calculation of the scattering length following the method described at the end of Subsection II D (see also below). In particular, the scattering length might be affected by states associated with the $H^+ + H(1s)$ ($F = 1$) channel which could predissociate into the open $H^+ + H(1s)$ ($F = 0$) continuum (type I predissociation; see Refs. 30, 31, 64, and 65). In the discussion of the $H^+ + H(1s)$ collision at ultralow temperatures, it is important to note that in the 0 K thermal limit of the $H^+ + H(1s)$ collision, only the H(1s, $F = 0$) level is populated so that only the $G = 1/2$ level correlated to this limit is relevant. One can, however, also determine s-wave scattering lengths for the $G = 1/2$ and $G = 3/2$ components of the upper $H^+ + H(1s, F = 1)$ dissociation limit. For the $G = 3/2$ component, our calculations give the same binding energy as reported in Refs. 19 and 20. Reference 20, however, assigns the corresponding state as a $G = 1/2$ state associated with the lower $[H^+ + H(1s, F = 0)]$ dissociation limit, which contradicts the correlation diagram presented in Fig. 1.

The $N = 0$ eigenphases [see Eq. (45)] are displayed as dashed lines (blue for $\tilde{\eta}_\alpha$ and magenta for $\tilde{\eta}_\beta$) in Fig. 8, where they are compared to the phase shifts η_{X^+} (full blue line) and η_{A^+} (full magenta line) obtained in a treatment neglecting the g/u mixing induced by the hyperfine interaction. The figure reveals the correspondence of the X^+ and A^+ $N = 0$ channels with the α and β channels, respectively [see discussion below Eq. (45)].

For $G = 1/2$, no π phase jumps of $\tilde{\eta}_{A^+}$ are detected between the two dissociation limits related to the two hyperfine components of the 1s level of the hydrogen atom. Consequently, there cannot be any $N = 0$ Feshbach resonances associated with the $H^+ + H(1s)$ ($F = 1$) collision channel. A closer inspection of Fig. 8 leads to the following additional conclusions:

- the X^+ s-wave scattering phase shift η_{X^+} is small and positive at low energies and first increases slightly before decreasing monotonically at higher energies,
- the A^+ s-wave scattering phase shift η_{A^+} is negative and falls off rapidly at low energies and then decreases with a similar slope as the X^+ phase shift at higher energies,
- the s-wave scattering eigenphase shift $\tilde{\eta}_\beta$ starts slightly above zero and shows a small increase before decreasing monotonically at higher energies and finally overlaps with the X^+ scattering phase shift η_{X^+}, and

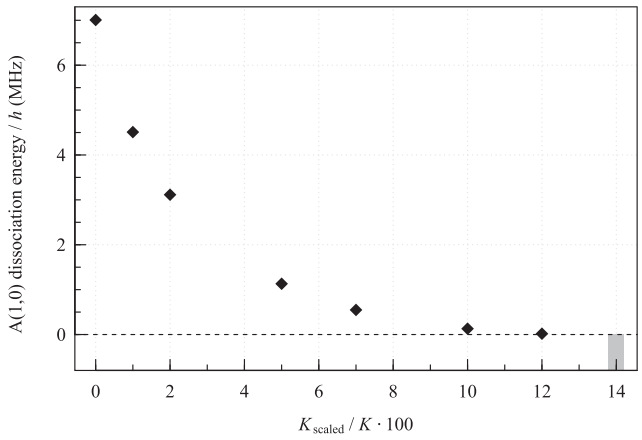


FIG. 7. Dissociation energies of the $A^+(1, 0)$ relative to the $H^+ + H(1s)$ ($F = 0$) dissociation limit as a function of the hyperfine-induced g/u coupling strength K_{scaled}. For K_{scaled} reaching 14% of its final value K in (27), no bound state could be detected anymore (indicated by the gray area).

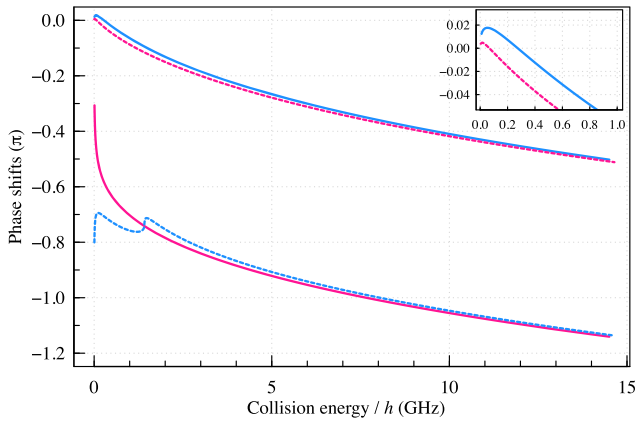


FIG. 8. Comparison of the s-wave scattering phases η_i (full lines) of the uncoupled X^+ (blue) and A^+ (magenta) channels and the eigenphases (dashed lines) $\tilde{\eta}_{A^+}$ (blue) and $\tilde{\eta}_{X^+}$ (magenta) channels in the treatment including the hyperfine interaction. The lines drawn in light color indicate the extrapolated limiting behavior at threshold. The collision energy is the energy with respect to the $H^+ + H(1s, F = 0)$ dissociation limit.

25 July 2026 18:11:09

- the s-wave scattering eigenphase shift $\tilde{\eta}_\alpha$ rises sharply at low energies, shows an oscillation at ≈1.4 GHz when the $F = 1$ channels opens, and then decreases monotonically at higher energies to become identical to the A^+ scattering phase shift η_{A^+}.

Consequently, we expect negative scattering lengths A_0 for channels with increasing phase shifts at zero energy (i.e., the X^+ and the α and β channels), whereas the channel with a decreasing phase shift at zero energy (i.e., the A^+ channel) should have a positive scattering length.

The scattering length is known to diverge in situations where a state is weakly bound or almost bound. This behavior is observed in Fig. 8, which compares the A^+ scattering phase shift η_{A^+} (full magenta line) with the scattering eigenphase shift $\tilde{\eta}_\alpha$ (dashed blue line). Both exhibit the same behavior at high energies, but the A^+ phase shift η_{A^+} converges to the next integer from below at zero energy, whereas $\tilde{\eta}_\alpha$ converges to the next lower integer from above. This behavior is in agreement with Levinson's theorem (see Ref. 66) that connects the zero-energy phase shift to the number of bound levels for a given rotational angular momentum. As is shown in Fig. 7, the $A^+(1, 0)$ level disappears when the hyperfine-induced g/u mixing is taken into account and, consequently, the $F = 0$ channel loses one bound state.

The elastic-collision cross section for a single-channel i is given by[67]

$$\sigma_i^{\mathrm{el}} = \frac{4\pi}{k_i^2} \sum_N^\infty (2N+1) \sin^2 \eta_i^{(N)}, \tag{46}$$

whereas the elastic ($\sigma_{ii}^{\mathrm{el}}$) and inelastic ($\sigma_{fi}^{\mathrm{r}}$) collision cross sections in multichannel problems are given by[67]

$$\sigma_{ii}^{\mathrm{el}} = \frac{\pi}{k_i^2} \sum_N^\infty (2N+1) \left|1 - S_{ii}^{(N)}\right|^2, \tag{47}$$

$$\sigma_{fi}^{\mathrm{r}} = \frac{\pi}{k_i^2} \sum_N^\infty (2N+1) \left|S_{fi}^{(N)}\right|^2. \tag{48}$$

At low collision energies, the sum over the partial waves N in the expressions above can be truncated because of the dominance of s-wave scattering ($N = 0$). The s-wave-scattering cross sections are depicted in Fig. 9 for the uncoupled scattering problem [i.e., for the X^+ (full blue line) and A^+ (full magenta line) channels] and after taking into account the hyperfine-induced g/u-symmetry breaking [i.e., for the $F = 0$ (dashed blue line) and $F = 1$ (dashed magenta line) channels]. Figure 9 also depicts the inelastic cross sections for spin excitation ($F = 0 \rightarrow F = 1$, full green line) and de-excitation ($F = 1 \rightarrow F = 0$, dashed green line). In the latter case, the cross section diverges at the $F = 1$ dissociation limit because k_2 in Eq. (48) approaches zero more rapidly than S_{12}. In the former case, this divergence does not occur because k_1 is finite at the $F = 1$ dissociation limit and $S_{12} = S_{21}$. The overall behavior of the cross sections displayed in Fig. 9 agrees with that reported in Ref. 5 for the lowest energies, where s-wave scattering dominates.

The s-wave scattering cross sections for the X^+ and A^+ channels have a sharp minimum at collision energies of

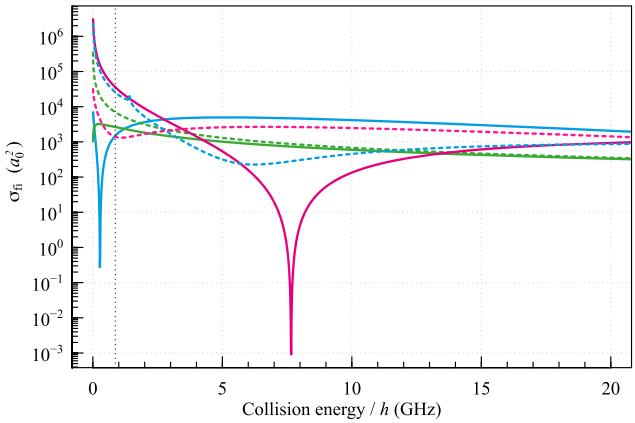


FIG. 9. Comparison of the elastic s-wave scattering cross sections σ_i^{el} (full lines) of the uncoupled X^+ (blue) and A^+ (magenta) channels and the elastic [$\sigma_{11}^{\mathrm{el}}$ ($F = 0$, blue dashed line) and $\sigma_{22}^{\mathrm{el}}$ ($F = 1$, magenta dashed line)] and inelastic [σ_{12}^{r} ($F = 1 \rightarrow F = 0$, dashed green line) and σ_{21}^{r} ($F = 0 \rightarrow F = 1$, full green line)] cross sections in the two-channel problem. The dotted vertical line indicates the top of the $N = 1$ centrifugal barrier. The collision energy for $\sigma_{11}^{\mathrm{el}}$ is given with respect to the $H^+ + H(F = 0)$ dissociation limit. For $\sigma_{22}^{\mathrm{el}}$, σ_{12}^{r}, and σ_{21}^{r}, it is given with respect to the $H^+ + H(F = 1)$ dissociation limit.

≈0.26 GHz and ≈7.65 GHz, respectively. Because the scattering phase shift of the X^+ state at zero energy is positive (corresponding to a negative scattering length), it crosses 0 (or a multiple of π) at low energies, which leads to a vanishing cross section according to Eq. (46). The zero-energy scattering phase shift of the A^+ channel is negative (corresponding to a positive scattering length) so that it crosses 0 (or a multiple of π) at higher energies. Because the contribution of higher partial waves to the total cross section at low energies is negligible (the vertical line in Fig. 9 indicates the energy corresponding to the top of the $N = 1$ centrifugal barrier), the total cross section becomes zero at ∼0.26 GHz in the X^+ channel. This behavior is known as the *Ramsauer effect*[68] and was first observed in the scattering of slow electrons with rare-gas atoms. For the A^+ channel, the minimum in the s-wave cross section occurs at higher energies, where higher partial waves are dominant so that the effect is strongly reduced.

The s-wave scattering length A_0 is determined by fitting the low-energy phase shift to the expression

$$k \cot \eta^{(N=0)} = -\frac{1}{A_0} + \frac{\pi\alpha}{6A_0^2} k + \frac{\alpha}{3A_0} k^2 \ln\left[\frac{\alpha k^2}{32}\right] + ck^2, \tag{49}$$

where $\alpha = 9/2$ is the polarizability of the ground state of the hydrogen atom[57] and c is a constant given in Ref. 69, where the effective-range theory was extended in order to include the effects of potentials that fall off as $1/R^4$. Because the proton–hydrogen-atom interaction potential also contains terms in $1/R^{n\geq 6}$, we determined c in a least-squares fit. The scattering lengths obtained in this way are summarized in Table III. We find good agreement in comparison with the values reported by Carbonell[19] for the scattering lengths calculated without considering the hyperfine interaction. The values reported by Glassgold,[21] Bodo *et al.*,[4] and Li and Gao[5] for the A^+ state are similar. When the hyperfine interaction is included, the scattering length changes sign and is reduced in magnitude by about 25%. It is important to note that the 0 K thermal limit of the $H^+ + H(1s)$ collision only involves the $F = 0$ ground state of

25 July 2026 18:11:09

TABLE III. Scattering lengths for the H^+–H collision (all values in atomic units) for the lower (X^+) and upper (A^+) states of H_2^+. If the hyperfine interaction is included (hfs, last line), the lower and the upper states correspond to a collision with the H(1s) ($F = 0$) and H(1s) ($F = 1$) state, respectively.

	Lower state	Upper state
Carbonell *et al.*[19]	−29.3	750(5)
Glassgold *et al.*[21]		801.2
Bodo *et al.*[4]	−28.8	725.2
Kaiser *et al.*[22]	−30.75(25)	762.8
Li and Gao[5] [a]	−30.371	810.52
This work (no hfs)	−29(2)	757(7)[b]
This work (hfs and g/u mixing, $G = 1/2$)	−578(6)	−43(4)

[a]The MQDT formalism of Ref. 5 could, in principle, be used to determine the scattering length for the $G = 1/2$ component.
[b]This value also corresponds to the $G = 3/2$ hyperfine component (see the text).

the H atom and thus corresponds to s-wave scattering between H^+ and H(1s, $F = 0$) with $G = 1/2$ and with scattering length −578(6) a_0.

The large change in the scattering cross section and scattering length upon including the g/u-symmetry-breaking part of the hyperfine interaction can also be deduced from the scattering wave function at zero energy, depicted in Fig. 10. For small k and $N = 0$, we obtain the relation

$$\phi(R) \propto \sin(kR)\cos\eta^{(0)} + \cos(kR)\sin\eta^{(0)} \propto R + \frac{\tan\eta^{(0)}}{k} \quad (50)$$

using the asymptotic expressions of the spherical Bessel functions. The scattering length A_0 is thus given by

$$A_0 = -\lim_{k\to 0}\frac{\tan\eta^{(0)}}{k}. \quad (51)$$

In Fig. 10, one sees that the wave function intersects the horizontal axis at $R > 0$ for the A^+ channel (blue) and at $R < 0$ for the $F = 0$ channel (magenta). The values of the scattering lengths indicated by the vertical lines are in agreement with the values given in Table III, which were obtained in a least-squares fit based on Eq. (49).

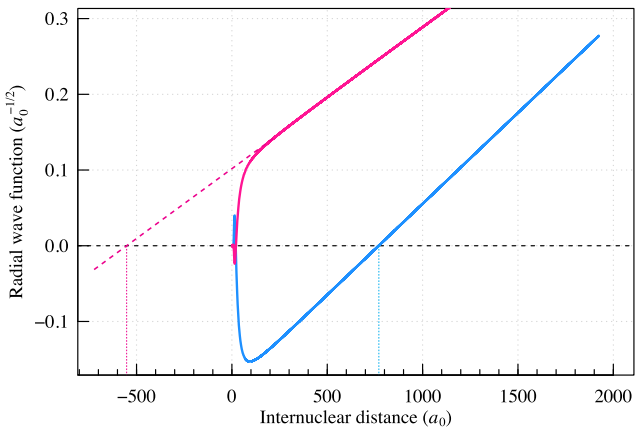


FIG. 10. Zero-energy wave function (calculated 0.02 MHz above the respective threshold) for the A^+ (blue) and the $F = 0$ (magenta) channel, respectively. The scattering length, given by the intersection of the zero-energy wave function with the R axis, is indicated by a vertical dotted line.

IV. CONCLUSIONS

The calculations presented in this article are the first to rigorously take into account the hyperfine interaction in the treatment of the elastic and inelastic proton–hydrogen-atom scattering. They demonstrate that the hyperfine interaction plays an important role in the structure and dynamics of H_2^+ near the $H^+ + H(1s)$ dissociation threshold. In particular, they prove that the $G = 1/2$ hyperfine component of the $A^+(v = 1, N = 0)$ level of H_2^+ does not exist, which has a large implication for the value of the $H^+ + H(1s)$ scattering length.

The calculations also revealed a very rich behavior that could in the future be studied experimentally, e.g., using cold, spin-polarized H atoms. Such atoms can be produced with a Zeeman decelerator.[70] The generation of cold samples of protons with densities sufficient for collision experiments, however, remains a challenge.

The procedure followed in our calculations can be generalized to any charge–hydrogen-atom or charge–anti-hydrogen-atom interaction. An example is the formation of the negative hydrogen ion

$$H + e^- \rightarrow H^- + h\nu, \quad (52)$$

which plays an important role in the formation of molecular hydrogen in the universe by associative detachment,[11]

$$H^- + H \rightarrow H_2 + e^-. \quad (53)$$

Another example, for which the cross section and scattering lengths are expected to be the same as those determined here, is the formation of the anti-hydrogen molecular ion ($\bar{H}_2^-$)

$$\bar{H}^- + \bar{H}(1s) \rightarrow \bar{H}_2^- + h\nu. \quad (54)$$

Although anti-molecules have not been produced yet, the current rapid improvements in sources of cold anti-protons and anti-hydrogen atoms (see, e.g., Refs. 71 and 72) are likely to make their synthesis possible in the coming years. The present results are relevant in this context, as well as in the discussion and modeling of the abundance of H_2 in the universe.[6,8,11,19,20]

ACKNOWLEDGMENTS

This work was financially supported by the Swiss National Science Foundation (Project No. 200020-172620) and the European Research Council (ERC) under the European Union's Horizon 2020 research and innovation programme (Advanced Grant No. 743121).

[1]D. R. Bates and A. Dalgarno, Proc. Phys. Soc. A **65**, 919 (1952).
[2]G. Hunter, B. F. Gray, and H. O. Pritchard, J. Chem. Phys. **45**, 3806 (1966).
[3]P. S. Krstić, J. H. Macek, S. Y. Ovchinnikov, and D. R. Schultz, Phys. Rev. A **70**, 042711 (2004).
[4]E. Bodo, P. Zhang, and A. Dalgarno, New J. Phys. **10**, 033024 (2008).
[5]M. Li and B. Gao, Phys. Rev. A **91**, 032702 (2015).
[6]D. R. Bates, Mon. Not. R. Astron. Soc. **111**, 303 (1951).
[7]D. R. Bates, K. Ledsham, and A. L. Stewart, Phil. Trans. R. Soc. London Ser. A **246**, 215 (1953).
[8]D. R. Bates, Astrophys. J. **270**, 564 (1983).
[9]P. C. Stancil, J. F. Babb, and A. Dalgarno, Astrophys. J. **414**, 672 (1993).
[10]J. F. Babb and K. P. Kirby, in *Molecular Astrophysics of Stars and Galaxies*, edited by T. W. Hartquist and D. A. Williams (Clarendon, Oxford, 1998), p. 11.

25 July 2026 18:11:09

[11]S. Lepp, P. C. Stancil, and A. Dalgarno, J. Phys. B: At., Mol. Opt. Phys. **35**, R57 (2002).
[12]A. Carrington, C. A. Leach, R. E. Moss, T. C. Steimle, M. R. Viant, and Y. D. West, J. Chem. Soc., Faraday Trans. **89**, 603 (1993).
[13]R. E. Moss, Chem. Phys. Lett. **206**, 83 (1993).
[14]P. R. Bunker and R. E. Moss, Chem. Phys. Lett. **316**, 266 (2000).
[15]A. D. J. Critchley, A. N. Hughes, and I. R. McNab, Phys. Rev. Lett. **86**, 1725 (2001).
[16]A. D. J. Critchley, A. N. Hughes, I. R. McNab, and R. E. Moss, Mol. Phys. **101**, 651 (2003).
[17]J. M. Peek, J. Chem. Phys. **50**, 4595 (1969).
[18]R. E. Moss, Mol. Phys. **80**, 1541 (1993).
[19]J. Carbonell, R. Lazauskas, D. Delande, L. Hilico, and S. Kiliç, Europhys. Lett. **64**, 316 (2003).
[20]J. Carbonell, R. Lazauskas, and V. I. Korobov, J. Phys. B: At., Mol. Opt. Phys. **37**, 2997 (2004).
[21]A. E. Glassgold, P. S. Krstić, and D. R. Schultz, Astrophys. J. **621**, 808 (2005).
[22]A. Kaiser, T.-O. Müller, and H. Friedrich, Mol. Phys. **111**, 878 (2013).
[23]H. J. Wörner, U. Hollenstein, and F. Merkt, Phys. Rev. A **68**, 032510 (2003).
[24]A. Osterwalder, A. Wüest, F. Merkt, and Ch. Jungen, J. Chem. Phys. **121**, 11810 (2004).
[25]C. A. Leach, M. S. Child, and D. E. Manolopoulos, Mol. Phys. **97**, 11 (1999).
[26]P. R. Bunker and P. Jensen, *Molecular Symmetry and Spectroscopy*, 2nd ed. (NRC, 1998).
[27]J. P. Pique, F. Hartmann, R. Bacis, S. Churassy, and J. B. Koffend, Phys. Rev. Lett. **52**, 267 (1984).
[28]J. P. Pique, F. Hartmann, S. Churassy, and R. Bacis, J. Phys. **47**, 1909 (1986).
[29]J. P. Pique, F. Hartmann, S. Churassy, and R. Bacis, J. Phys. **47**, 1917 (1986).
[30]M. Broyer, J. Vigué, and J. C. Lehmann, J. Phys. **39**, 591 (1978).
[31]J. Vigué, M. Broyer, and J. C. Lehmann, J. Phys. **42**, 937 (1981).
[32]M. Beyer and F. Merkt, Phys. Rev. Lett. **116**, 093001 (2016).
[33]M. Beyer and F. Merkt, Phys. Rev. X **8**, 031085 (2018).
[34]A. J. Moerdijk and B. J. Verhaar, Phys. Rev. A **51**, R4333 (1995).
[35]E. R. I. Abraham, W. I. McAlexander, H. T. C. Stoof, and R. G. Hulet, Phys. Rev. A **53**, 3092 (1996).
[36]H. Wang, A. N. Nikolov, J. R. Ensher, P. L. Gould, E. E. Eyler, W. C. Stwalley, J. P. Burke, J. L. Bohn, C. H. Greene, E. Tiesinga, C. J. Williams, and P. S. Julienne, Phys. Rev. A **62**, 052704 (2000).
[37]K. Pachucki and J. Komasa, Phys. Rev. A **83**, 042510 (2011).
[38]Z. Idziaszek, A. Simoni, T. Calarco, and P. S. Julienne, New J. Phys. **13**, 083005 (2011).
[39]M. Beyer and F. Merkt, J. Mol. Spectrosc. **330**, 147 (2016).
[40]R. Jaquet and W. Kutzelnigg, Chem. Phys. **346**, 69 (2008).
[41]R. Jaquet and M. V. Khoma, Mol. Phys. **110**, 669 (2012).
[42]P. Quadrelli, K. Dressler, and L. Wolniewicz, J. Chem. Phys. **92**, 7461 (1990).
[43]A. Carrington and R. A. Kennedy, in *Ions and Light*, edited by M. T. BOWERS (Academic Press, 1984), pp. 393–442.
[44]G. Hunter and H. O. Pritchard, J. Chem. Phys. **46**, 2146 (1967).
[45]W. Kolos and L. Wolniewicz, Rev. Mod. Phys. **35**, 473 (1963).
[46]R. N. Zare, *Angular Momentum* (John Wiley & Sons, New York, 1988).
[47]L. Wolniewicz and J. D. Poll, J. Mol. Spectrosc. **72**, 264 (1978).
[48]B. R. Johnson, J. Chem. Phys. **69**, 4678 (1978).
[49]F. T. Smith, Phys. Rev. **179**, 111 (1969).
[50]F. H. Mies, Mol. Phys. **41**, 953 (1980).
[51]B. R. Johnson, J. Chem. Phys. **67**, 4086 (1977).
[52]B. R. Johnson, J. Comput. Phys. **13**, 445 (1973).
[53]B. R. Johnson, Phys. Rev. A **32**, 1241 (1985).
[54]V. I. Korobov, L. Hilico, and J.-Ph. Karr, Phys. Rev. A **74**, 040502(R) (2006).
[55]D. Sprecher, C. Jungen, and F. Merkt, J. Chem. Phys. **140**, 104303 (2014).
[56]P. J. Mohr, D. B. Newell, and B. N. Taylor, J. Phys. Chem. Ref. Data **45**, 043102 (2016).
[57]H. A. Bethe and E. E. Salpeter, *Quantum Mechanics of One-and Two-Electron Atoms* (Springer Verlag, 1957), p. 101.
[58]R. A. Frosch and H. M. Foley, Phys. Rev. **88**, 1337 (1952).
[59]R. L. Cook and F. C. De Lucia, Am. J. Phys. **39**, 1433 (1971).
[60]R. M. Herman and A. Asgharian, J. Mol. Spectrosc. **19**, 305 (1966).
[61]P. R. Bunker and R. E. Moss, Mol. Phys. **33**, 417 (1977).
[62]A. U. Hazi, Phys. Rev. A **19**, 920 (1979).
[63]C. A. Coulson, Proc. R. Soc. Edinburgh Sect. A **61**, 20 (1941).
[64]J. Vigué, M. Broyer, and J. C. Lehmann, J. Phys. **42**, 949 (1981).
[65]J. Vigué, M. Broyer, and J. C. Lehmann, J. Phys. **42**, 961 (1981).
[66]C. J. Joachain, *Quantum Collision Theory* (North Holland, 1975).
[67]L. D. Landau and E. M. Lifshitz, *Quantum Mechanics: Non-Relativistic Theory* (Pergamon, London, 1981).
[68]C. Ramsauer, Ann. Phys. **369**, 513 (1921).
[69]T. F. O'Malley, L. Spruch, and L. Rosenberg, J. Math. Phys. **2**, 491 (1961).
[70]S. D. Hogan, A. W. Wiederkehr, M. Andrist, H. Schmutz, and F. Merkt, J. Phys. B: At., Mol. Opt. Phys. **41**, 081005 (2008).
[71]N. Madsen, Phil. Trans. R. Soc. A **368**, 3671 (2010).
[72]M. Doser, S. Aghion, C. Amsler, G. Bonomi, R. S. Brusa, M. Caccia, R. Caravita, F. Castelli, G. Cerchiari, D. Comparat, G. Consolati, A. Demetrio, L. D. Noto, C. Evans, M. Fanì, R. Ferragut, J. Fesel, A. Fontana, S. Gerber, M. Giammarchi, A. Gligorova, F. Guatieri, S. Haider, A. Hinterberger, H. Holmestad, A. Kellerbauer, O. Khalidova, D. Krasnický, V. Lagomarsino, P. Lansonneur, P. Lebrun, C. Malbrunot, S. Mariazzi, J. Marton, V. Matveev, Z. Mazzotta, S. R. Müller, G. Nebbia, P. Nedelec, M. Oberthaler, N. Pacifico, D. Pagano, L. Penasa, V. Petracek, F. Prelz, M. Prevedelli, B. Rienaecker, J. Robert, O. M. Rohne, A. Rotondi, H. Sandaker, R. Santoro, L. Smestad, F. Sorrentino, G. Testera, I. C. Tietje, E. Widmann, P. Yzombard, C. Zimmer, J. Zmeskal, and N. Zurlo, Phil. Trans. R. Soc. A **376**, 20170274 (2018).

25 July 2026 18:11:09